Global Journal of Pure and Applied Mathematics.
ISSN 0973-1768 Volume 20, Number 4 (2024), pp. 657-675

https://dx.doi.org/10.37622/GJPAM/20.4.2024.657-675

Heat Transfer Characteristics of Williamson Nanofluid Flow past a Horizontal Surface with Binary Chemical Reaction and Activation Energy

[1]Y. Veeranna , [2]B.S. Prathibha, [3]P. B. Sampath Kumar*

[1]Department of Studies and Research in Mathematics, Government Science College (Autonomous), Bengaluru-560 001, Karnataka, India.
[2]Government SriKrishnarajendra Silver Jubilee Technological Institute, Bangalore- 560 001, Karnataka, India.
[3]Department of Mathematics, PG Centre Ramanagara, Bangalore University, Ramanagara-562159, Karnataka, India.*

Abstract

In this era of modern science, non-Newtonian nanofluids have gained much importance in research due to large-scale applications in science and engineering. Hence, our investigation centres on utilizing Williamson Nanofluid to improve heat transfer across a horizontal surface, while examining the impacts of magnetic fields, solar radiation, chemical reactions, and activation energy. The nanofluid model integrates thermophoresis and Brownian motion to account for their combined effects in the energy transport equation. The numerical solutions address relevant boundary value problems by employing the shooting technique. The results are then illustrated through graphs and tables, providing insights into the distinctive features of various flow fields within the working fluid. The numerical computations consider two distinct scenarios: Williamson nanofluid and ordinary Williamson fluid. The findings indicate a higher heat transfer rate for the Williamson nanofluid than the ordinary Williamson fluid.

Keywords: Numerical solution, Williamson nanofluid, solar radiation, chemical reaction, activation energy.

Introduction

In modern research, understanding the mechanisms of non-Newtonian materials has become a focal point. The rheological characteristics of non-Newtonian materials significantly differ from those of Newtonian materials. Various substances such as shampoos, toothpaste, soaps, honey, sugar solutions, polymers, blood, ketchup, applesauce, drilling muds, and lubricants fall under the category of non-Newtonian fluids. All these liquids exhibits various rheological properties and mechanisms. In non-Newtonian fluids, pseudoplastic fluids stand out as among the most commonly encountered types. The Williamson fluid represents a pseudoplastic type of non-Newtonian fluid characterized by shear-thinning behavior. The Williamson fluid holds significant importance due to its applications in various fields including lubricants, biomedical fluids, emulsions, and nuclear fuel slurries. Williamson [1] explained the flow behavior of pseudoplastic materials and introduced a model to describe their characteristic flow. Experimental validation confirmed, the viscosity decrease with increasing rate of shear stress. Lyubimov and Perminov [2] investigated the effects of gravitational force on a thin layer of Williamson fluid. Nadeem et al. [3] formulated a model where they considered chyme as a Williamson fluid, and they conducted the flow analysis within the annular region created by two concentric tubes. Vajravelu and Dhivya [4] conducted a numerical analysis of Williamson fluid flow over a moving vertical cylinder with variable porosity using the Crank-Nicholson method. Salawu [5] numerically analyzed the stagnation-point flow with considering the influence of activation energy within a Williamson fluid comprising tiny particles over an expansive plate.

The present study investigates the MHD flow of a Williamson nanofluid across an exponential stretching surface, taking into account nonlinear thermal radiation to enhance heat transfer. While stretching scenarios have been extensively analyzed with linear thermal radiation, there has been limited attention given to flow situations involving nonlinear thermal radiation. However, the impact of thermal radiation plays a crucial role in influencing the heat transfer rate and temperature distributions within the boundary layer flow of the participating fluid. This phenomenon finds various practical applications in industries such as metallurgy, manufacturing, and energy generation. Additionally, it holds significance in electronics by impacting the performance and cooling of electronic components. Notably, one of the most notable practical uses of this concept is in utilizing solar radiation as an energy source on Earth. The study conducted by Rashidi et al. [6] examined the MHD stretched flow of a nanofluid under the influence of buoyancy and thermal radiation. A salient feature of thermal radiation in nanofluid unsteady flow over a stretching sheet was reported by Das et al. [7], the study examined the impact of thermal radiation in a time-dependent magnetohydrodynamic flow with varying viscosity. Mahanthesh et al. [8] conducted an investigation into the radiative flow of a hydromagnetic nano-fluid over the rotation of a disk. Their analysis included a nano-fluid composed of water-based nanoparticles, considering various shapes of nanoparticles such as lamina, column, sphere, tetrahedron, and hexahedron. Khan et al [9] explored a mathematical model for entropy generation incorporating variable fluid properties. They further examined the impact of mixed convection and nonlinear radiation. Reddy et al. [10] conducted a comprehensive examination of radiative heat transfer in Casson nanofluid, while also considering the viscous dissipation and particle movement. Moreover, recent research efforts have expanded beyond examining individual components to provide a complete understanding of thermal radiation's influence on various flows [11-18]. These studies provide a comprehensive understanding of the various impacts of thermal radiation in diverse fluid dynamics situations.

The motion of Williamson liquid combined with chemical reactions has found extensive applications in various fields such as drying processes, geothermal reservoirs, surface dehydration, enhanced oil recovery, geothermal pools, fibrous insulation, food processing, thermal insulation, iron rusting, fog formation, nuclear reactor cooling, synthetic materials, and numerous others. Due to extensive applications, the consequence of chemical reaction has been investigated and reported by many researchers Mukhopadhyay et al [19], Hayat et al. [20], Umavathi et al. [21], Mustafa et al. [22], Majeed et al. [23] and Nadeem et al [24].

Common liquids are often underutilized in various scientific and technical sectors due to their poor heat conductivity. However, nanoparticles are gaining significant attention in this era due to their remarkable thermal impact and unique applications across industries, biological, and engineering sectors. Such as nuclear power, paper production, insolation collectors, glass-fibre manufacture, geothermal energy pipe cooling systems, and heat transmission in aircraft apparatus. Nanoparticles, characterized by their small metallic particles ranging from 1 to 100 nm, possess enhanced thermo-physical properties. Recent studies have highlighted that nanofluids exhibit higher thermal conductivity compared to conventional fluids. Choi [25] provided experimental validation of nanofluids, establishing the existence of this concept. Throughout the last two decades, researchers around the world have been fascinated by the exceptional properties of nanofluid, remarkable studies being recorded in the field [26-34].

The current study investigates the utilization of Williamson Nanofluid to enhance heat transfer across a horizontal surface, while simultaneously analyzing the effects of magnetic fields, solar radiation, chemical reactions, and activation energy. The presenting governing equations are highly nonlinear mathematical expressions that are numerically treated to examine the outcomes. Graphical representations are employed and discussed to express the mechanisms underlying various physical constraints on dimensionless quantities. The numerical computations cover two distinct scenarios: Williamson nanofluid and ordinary Williamson fluid. The results reveal a notably higher heat transfer rate for the Williamson nanofluid in comparison to the ordinary Williamson fluid.

Mathematical Formulation

We examine a steady two-dimensional flow of Williamson fluid over an exponentially stretching surface in the presence of nanoparticles. The flow configuration and coordinate system are illustrated in Figure 1. The x-axis aligns with the stretching surface in the direction of fluid flow, while the y-axis is orthogonal to it. The surface is exponentially stretched in the x-direction with a velocity $U_w(x) = U_0 e^{x/L}$. A magnetic field strength B_0 is applied along the y-direction. At the surface, the temperature and nanoparticle volume fraction of the nanofluid are denoted as T_w and C_w, respectively.

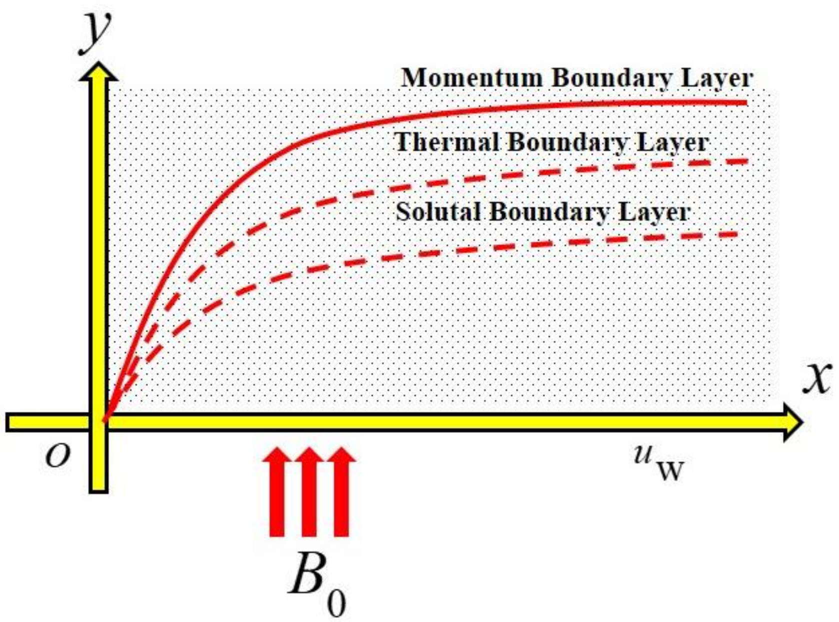

Figure 1: Physical model and coordinate system.

With all above assumptions the governing boundary layer equations are:

$$\frac{\partial u}{\partial x} + \frac{\partial v}{\partial y} = 0, \tag{1}$$

$$u\frac{\partial u}{\partial x} + v\frac{\partial u}{\partial y} = \nu\frac{\partial^2 u}{\partial y^2} + \sqrt{2}\nu\Gamma\frac{\partial u}{\partial y}\frac{\partial^2 u}{\partial y^2} - \frac{\sigma B_0^2}{\rho}u - \frac{\nu}{k'}u, \tag{2}$$

$$u\frac{\partial T}{\partial x} + v\frac{\partial T}{\partial y} = \alpha_m\frac{\partial^2 T}{\partial y^2} + \tau\left[D_m\frac{\partial C}{\partial y}\frac{\partial T}{\partial y} + \frac{D_T}{T_\infty}\left(\frac{\partial T}{\partial y}\right)^2\right] + \frac{Q_0}{\rho c_p}(T - T_\infty) - \frac{1}{\rho c_p}\frac{\partial q_r}{\partial y}, \tag{3}$$

$$u\frac{\partial C}{\partial x} + v\frac{\partial C}{\partial y} = D_m\frac{\partial^2 C}{\partial y^2} + \frac{D_T}{T_\infty}\frac{\partial^2 T}{\partial y^2} - k_r^2(C - C_\infty)\left(\frac{T}{T_\infty}\right)^m \exp\left(-\frac{E_a}{\kappa T}\right), \tag{4}$$

The radiative heat flux expression in equation (3) is given by the Rosseland approximation as;

$$q_r = -\frac{4\sigma^*}{3k^*}\frac{\partial T^4}{\partial y} = -\frac{16\sigma^*}{3k^*}T^3\frac{\partial T}{\partial y}, \tag{5}$$

Where σ^* and k^* are the Stefan-Boltzman constant and the mean absorption coefficient correspondingly, and in view to equation (5) in equation (3) reduces to

$$u\frac{\partial T}{\partial x}+v\frac{\partial T}{\partial y}=\alpha_m\frac{\partial^2 T}{\partial y^2}+\tau\left[D_m\left(\frac{\partial C}{\partial y}\frac{\partial T}{\partial y}\right)+\frac{D_T}{T_\infty}\left(\frac{\partial T}{\partial y}\right)^2\right]+\frac{Q_0}{\rho c_p}(T-T_\infty)$$
$$+\frac{16\sigma^*}{3\rho c_p k^*}\left[T^3\frac{\partial^2 T}{\partial y^2}+3T^2\left(\frac{\partial T}{\partial y}\right)^2\right] \qquad \textbf{(6)}$$

The boundary conditions considered for the present flow analysis are;

$$u=U_w(x)=U_0e^{x/L},\quad v=0,\quad T=T_w,\quad C=C_w \quad \text{at} \quad y=0,$$
$$u=0,\quad T\to T_\infty,\quad C\to C_\infty \quad as \quad y\to\infty. \qquad \textbf{(7)}$$

The term $k_r^2(C-C_\infty)\left(\frac{T}{T_\infty}\right)^m\exp\left(-\frac{E_a}{\kappa T}\right)$ in equation (4) represents the modified Arrhenius equation in which k_r^2 is the reaction rate, E_a the activation energy, $\kappa=8.61\times10^{-5}eV/K$ the Boltzmann constant and m the fitted rate constant which generally lies in the range $-1<m<1$. where u and v are velocity components along x and y directions respectively, T and C are temperature and volume fraction of nanoparticles correspondingly, ν -kinematic viscosity, ρ -is density of the fluid, Q_0-dimensional heat source coefficient, B_0 -magnetic field, k' -permeability of the porous medium, $\alpha_m=k/\rho c_p$ -thermal diffusivity of the fluid, k -thermal conductivity of the fluid, D_T -thermophoretic diffusion coefficient, D_m -Brownian diffusion coefficient, $\tau=(\rho c)_p/(\rho c)_f$ -ratio of the effective heat capacity of the nanoparticle to that of an ordinary fluid, $(\rho c)_f$ and $(\rho c)_p$ are heat capacities of the ordinary fluid and nanoparticles respectively, T_∞ and C_∞ are ambient temperature and volume fraction of nanoparticles respectively and q_r radiative heat flux.

Now, introduce the following similarity transformations

$$u=U_0e^{\frac{x}{L}}f'(\eta),\, v=-\sqrt{\frac{U_0\nu}{2L}}e^{\frac{x}{2L}}\big(f(\eta)+\eta f'(\eta)\big),\, \eta=\sqrt{\frac{U_0}{2\nu L}}e^{x/2L}y$$
$$T=\theta(\eta)(T_w-T_\infty)+T_\infty,\, C=\phi(\eta)(C_w-C_\infty)+C_\infty \qquad \textbf{(8)}$$

With the help of above transformations, equation Eq. (1) is identically satisfied and Equation's. (2), (4) and (6) along with boundary conditions (7) take the following equations;

$$f'''+ff''-2(f')^2+\lambda f''f'''-(M+kp)f'=0, \qquad \textbf{(9)}$$
$$\theta''+R\left[\big(1+(\theta_w-1)\theta(\eta)\big)^3\theta''(\eta)+3(\theta_w-1)\theta'^2(\eta)\big(1+(\theta_w-1)\theta(\eta)\big)^2\right]$$
$$+\Pr\{f\theta'+Nb\phi'\theta'+Nt(\theta')^2+\mathrm{Q}\theta\}=0, \qquad \textbf{(10)}$$
$$\phi''+Lef\phi'+\frac{Nt}{Nb}\theta''-Le\sigma(1+\delta\theta)^m\phi\exp\left(-\frac{E}{1+\delta\theta}\right)=0, \qquad \textbf{(11)}$$

and the corresponding boundary conditions become;

$$f(0)=0,\ f'(0)=1,\ \theta(0)=1,\ \phi(0)=1,$$
$$f'(\infty)=0,\ \theta(\infty)=0,\ \phi(\infty)=0. \qquad \textbf{(12)}$$

where $\omega = \Gamma\sqrt{\frac{U_0^3 e^{3x/L}}{\nu L}}$ -Williamson fluid Parameter, $M = \frac{2L\sigma B_0^2}{\rho U_w}$ -magnetic field parameter, $kp = \frac{2L\nu}{k' U_w}$ -porous parameter, $Pr = \frac{\nu}{\alpha_m}$ -Prandtl number, $R = \frac{16\sigma^* T_\infty^3}{3kk^*}$ -radiation parameter, $\theta_w = \frac{T_w}{T_\infty}$ -temperature parameter, $Nb = \frac{D_m(C_w - C_\infty)}{\nu}$ -Brownian motion parameter, $Nt = \frac{\tau D_T(T_w - T_\infty)}{T_\infty \nu}$ -thermophoresis parameter, $Le = \frac{\nu}{D_m}$ -Lewis number and $Q = \frac{Q_0 2L}{\rho c_p U_w}$ –heat generation parameter, $\sigma = -\frac{k_r^2 2L}{U_w}$ -dimensionless reaction rate, $\delta = \frac{T_w - T_\infty}{T_\infty}$ - the temperature difference parameter, $E = \frac{E_a}{\kappa T_\infty}$ - non-dimensional activation energy.

The Skin friction coefficient, Nusselt number and Sherwood numbers are;

$$C_f = \frac{\tau_w}{\rho U_w^2}, \quad Nu_x = \frac{x q_w}{k(T_w - T_\infty)}, \quad Sh_x = \frac{x q_m}{D_B(C_w - C_\infty)} \tag{13}$$

Where τ_w -surface shear stress, q_w-surface heat flux and q_m -surface mass flux are given by;

$$\tau_w = \mu\left(\frac{\partial u}{\partial y} + \frac{\Gamma}{2}\left(\frac{\partial u}{\partial y}\right)^2\right)_{y=0},$$

$$q_w = -k\left(\frac{\partial T}{\partial y} + q_r\right)_{y=0},$$

$$q_m = -D_m\left(\frac{\partial c}{\partial y}\right)_{y=0}. \tag{14}$$

Now through merging equation (8) and (14) in interpretation of equation (13), we have obtained;

$$\sqrt{Re_x}C_f = \left(f''(0) + \frac{\lambda}{2}f''(0)^2\right),$$

$$\frac{Nu_x}{\sqrt{2Re}} = -\frac{x}{2L}(1 + R\theta_w^3)\theta'(0),$$

$$\frac{Sh_x}{\sqrt{2Re}} = -\frac{x}{2L}\phi'(0). \tag{15}$$

Where $Re_x = \frac{U_0 L}{\nu}$ is the local Reynolds number.

Physical Interpretation

In this section, we conducted comprehensive numerical simulations across coupled values of pertinent physical parameters, including velocity $(f'(\eta))$, temperature $(\theta(\eta))$, nanoparticle volume fraction $(\phi(\eta))$, skin friction coefficient $(C_f Re_x^{0.5})$, Nusselt number $(Nu_x/(2Re_x)^{0.5})$ and Sherwood number $(Sh_x/(2Re_x)^{0.5})$. We elucidate and discuss the physical implications of the numerical outcomes through plotted figures and tables. The default values for the parameters in our numerical simulations are explicitly indicated in each figure. Moreover, we present graphical representations of various physical parameters in two distinct cases: one pertaining to the non-Newtonian fluid scenario (Williamson fluid), and the other involving the non-Newtonian nanofluid (Williamson nanofluid case).

Figure 2 and 3 is demonstrates the temperature $\theta(\eta)$ and volume fraction profile $\phi(\eta)$ for different type of fluids. It is observed that, the temperature of Williamson nanofluid is higher than that of Newtonian-nano, Williamson and Newtonian fluid in order. It is note that the Williamson nanofluid have more capable in heating process. Figure 4 is drawn to determine the impact of R on Nusselt number $(Nu_x/(2Re_x)^{0.5})$ versus Q. The $Nu_x/(2Re_x)^{0.5}$ slightly decreases for larger Q and increases for larger R in both cases. The impact of R vs Q on Sherwood number $(\mathrm{Sh_x}/(2Re_x)^{0.5})$ is plotted in figure 5. The $\mathrm{Sh_x}/(2Re_x)^{0.5}$ enhanced for higher R and Q. The mass transfer rate is suddenly rises for larger heat source Q in case of nanofluid model than ordinary fluid. Figure 6 is drawn to determine the impact of σ on $\mathrm{Sh_x}/(2Re_x)^{0.5}$ versus E. The $\mathrm{Sh_x}/(2Re_x)^{0.5}$ enhanced for σ and decreases for E. It is also noted that, the Williamson nanofluid have high mass transfer rate than Williamson fluid.

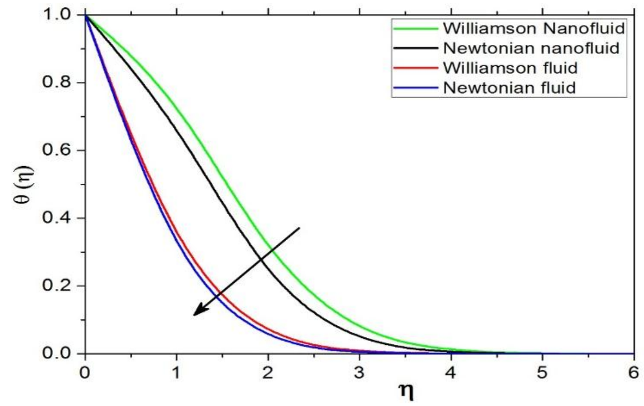

Figure 2: Variation of temperature profile.

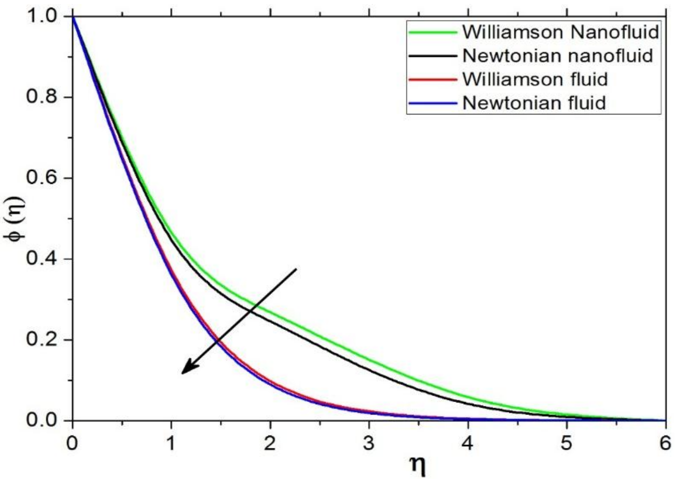

Figure 3: Variation of concentration profile.

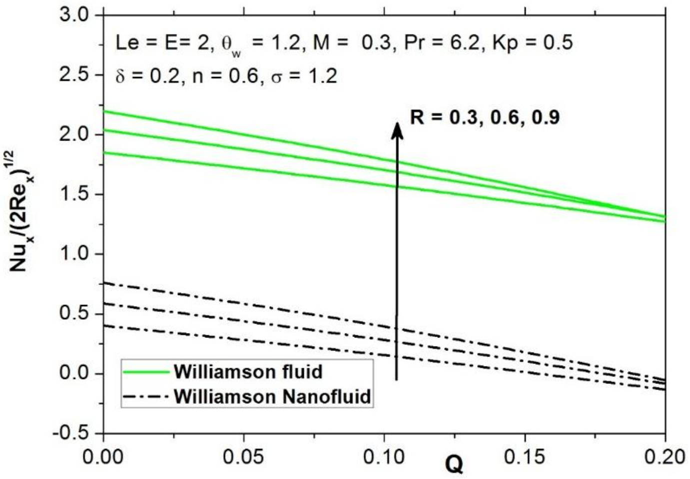

Figure 4: Nusselt number for radiation and heat source parameter.

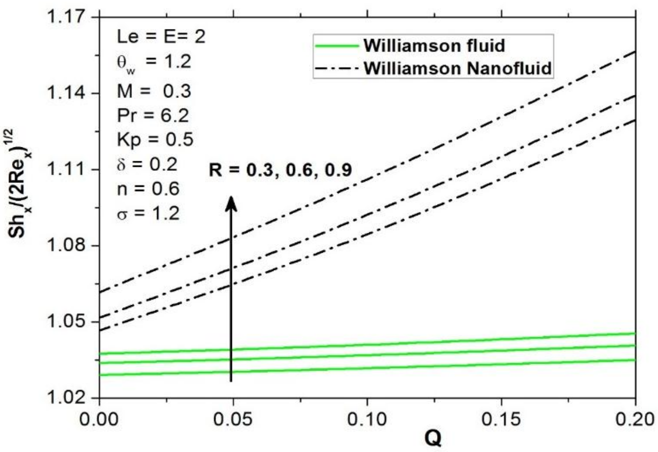

Figure 5: Sherwood number for radiation and heat source parameter.

Figure 7 illustrates the impact of K_p on $f'(\eta)$. It is evident that the presence of a porous medium imposes significant resistance to the liquid flow, thereby decelerating its motion. Consequently, as K_p increases, the resistance to liquid flow intensifies, leading to a reduction in velocity. Figures 8 and 9 depict the variations of $\theta(\eta)$ and $\phi(\eta)$ for K_p, respectively. In both the Williamson and Williamson nanofluid cases, $\theta(\eta)$ and $\phi(\eta)$ exhibit a monotonous increase with increasing K_p. The presence of porous disturbances in liquid motion, coupled with continuous heat supply to the liquid at a uniform temperature T_w on the surface, results in enhanced liquid temperatures. Additionally, the associated boundary layer thickness is higher in the nanoliquid model compared to the ordinary liquid case.

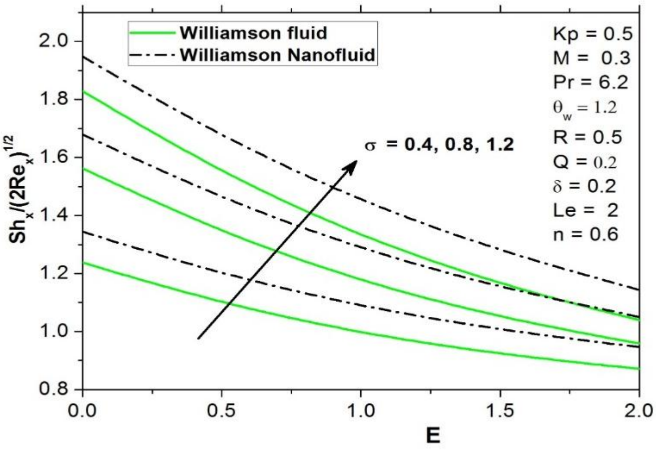

Figure 6: Sherwood number for reaction rate and activation energy parameter.

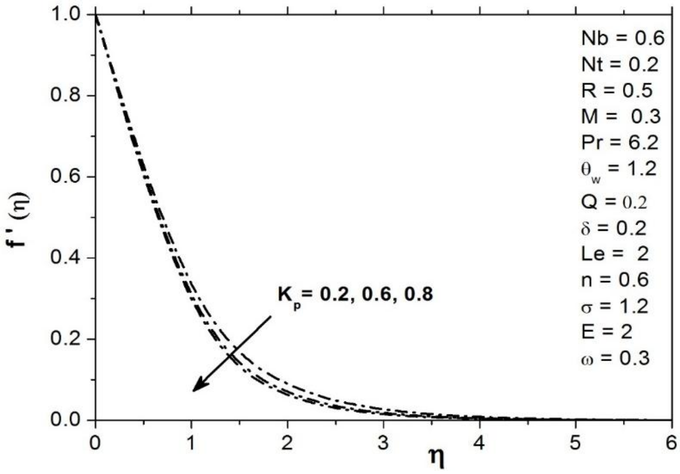

Figure. 7. Velocity profile for permeability parameter

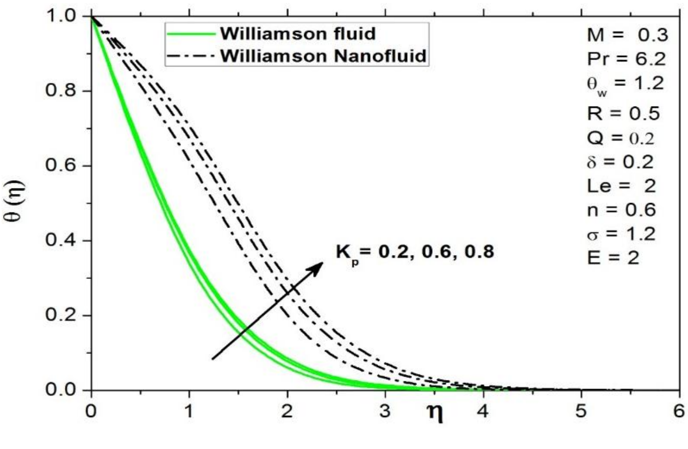

Figure 8: Temperature profile for permeability parameter

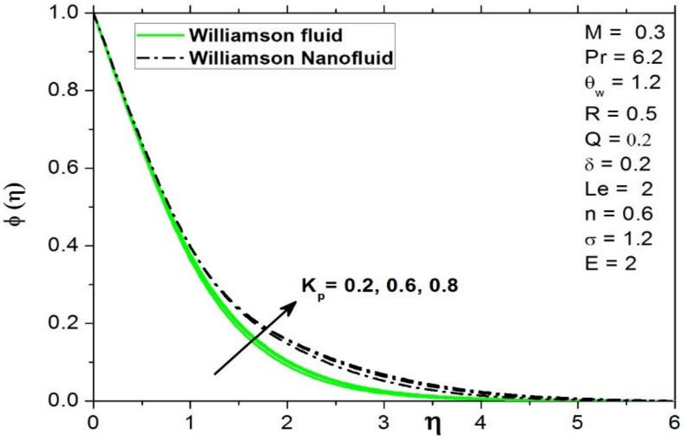

Figure 9: Concentration profile for permeability parameter

The variation of temperature difference parameter δ on $\phi(\eta)$ is plotted in figure 10. It is noted that the higher values of δ is diminishes $\phi(\eta)$ in both cases. The reason behind that, the higher δ $(= (T_f - T_\infty)/T_\infty$) increases the wall temperature and decreases the ambient temperature. However, the liquid concentration decrease. Figure 11 represent the $\phi(\eta)$ for various values of E. It is reported that the impact of activation energy E leads to increases in $\phi(\eta)$. Due to higher values of E leads to lesser reaction rate constant and consequently slow down the chemical reaction, as a result increases in $\phi(\eta)$. The impact σ on $\phi(\eta)$ is illustrated in figure 12. We can see that diminishing in volume fraction profile when σ is increased. Physically, an higher σ generates the greater reaction rate then random motion of nanoparticles rate decreases, as result reduction accurse in $\phi(\eta)$. Also, solute boundary layer thickness is higher in case nanoliquid model than ordinary liquid.

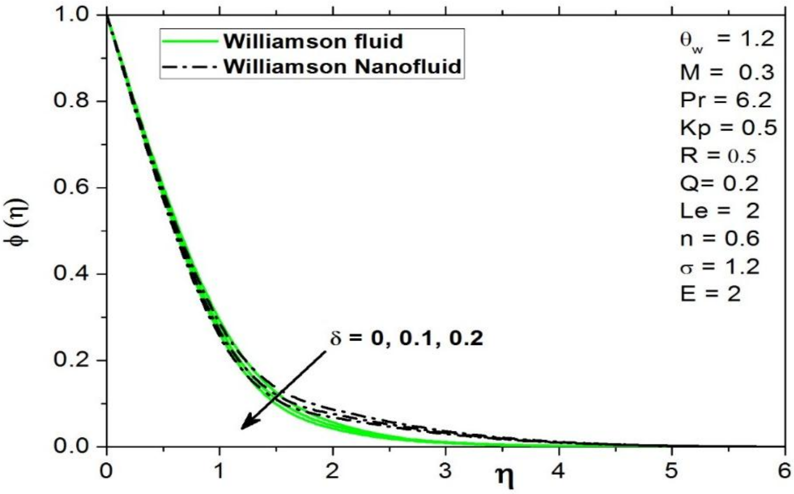

Figure 10: Concentration profile for temperature difference parameter

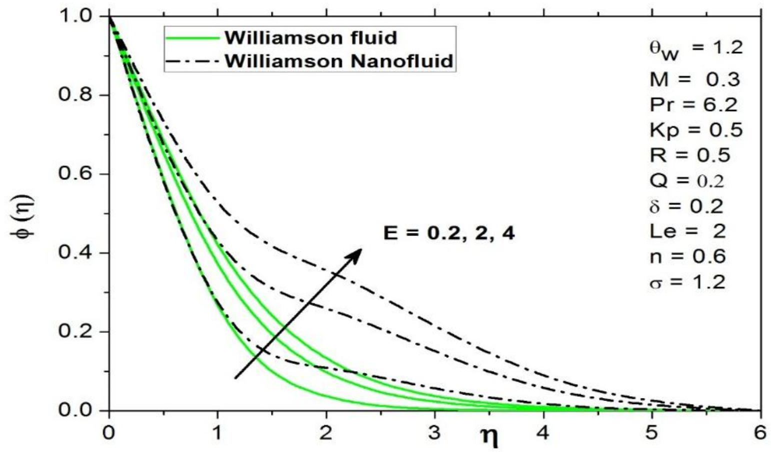

Figure 11: Concentration profile for activation energy parameter

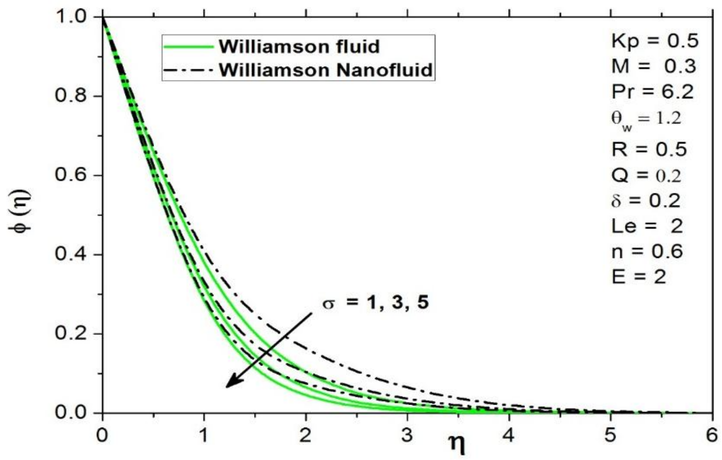

Figure 12: Concentration profile for chemical reaction rate parameter

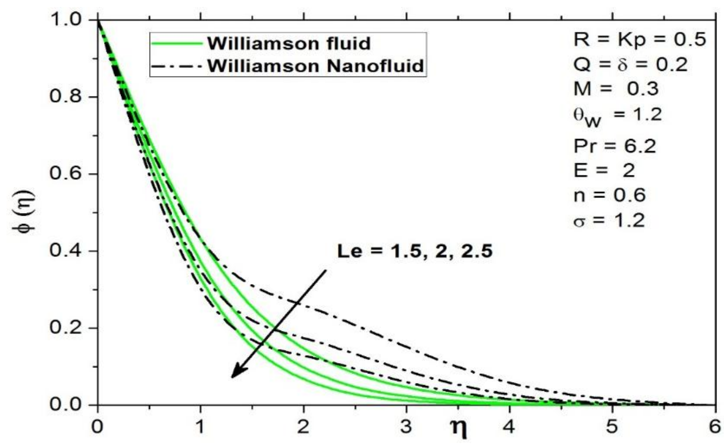

Figure 13: Concentration profile for Lewis number

Figure 13 shows the effect of the Lewis number Le on $\phi(\eta)$. The higher Lewis number decrease the Brownian diffusion coefficient. The lower solute diffusivity slow down the nanoparticles motion, while volume fraction profile decreases for the higher Le in both cases. Figure 14-17 describes the temperature profile for Nb, Nt, R and θ_w. Increases in parametric (Nb, Nt, R and θ_w) values leads to increase in liquid temperature along with their thermal boundary layer thickness. Behaviour of Q_t on temperature field $\theta(\eta)$ is depicted in figure 18. In both cases Williamson fluid and Williamson nanofluid. It is noted that, the liquid temperature is augmented via higher values of Q_t in both Williamson fluid and Williamson nanofluid cases. By enhancing the values of Q_t provides extra heat from surface towards working fluid, in fact the fluid temperature and their related thermal boundary layer thickness is increase. It is worth to mention that, the nanoliquid model (Williamson nanofluid) is more effective in flow field characteristics than ordinary liquid (Williamson fluid).

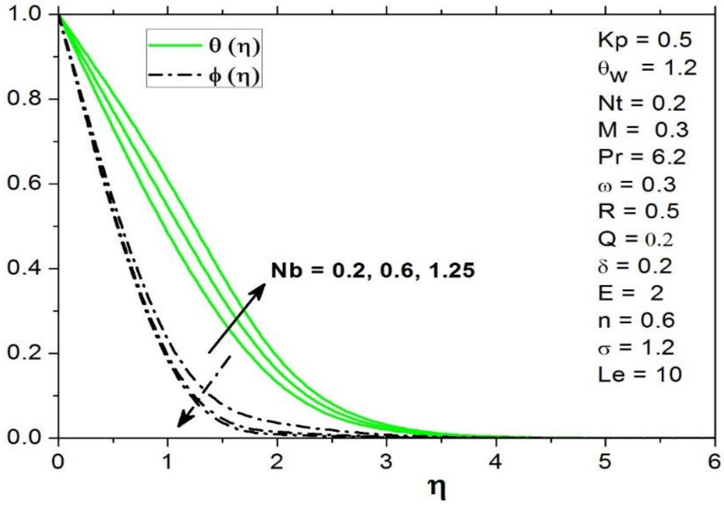

Figure 14: Temperature and concentration profile for Brownian motion parameter.

Table 1 presents the numeric data of $Nu_x/(2Re_x)^{0.5}$ and $Sh_x/(2Re_x)^{0.5}$ for different values of $E, Le, \sigma, \delta, R, \theta_w$ and Q. The $Nu_x/(2Re_x)^{0.5}$ decreases for E, Le and increases for σ, δ in nanofluid model but no variations can be observed in ordinary fluid model. Significantly rises the heat and mass transfer rate when increase in R, δ and θ_w. The reverse effect is observed in $Nu_x/(2Re_x)^{0.5}$ and $Sh_x/(2Re_x)^{0.5}$ for Q. It is also observed that, the mass transfer rate ($Sh_x/(2Re_x)^{0.5}$) is more in Williamson nanofluid case than Williamson fluid but quit opposite behaviour can be observed in heat transfer process.

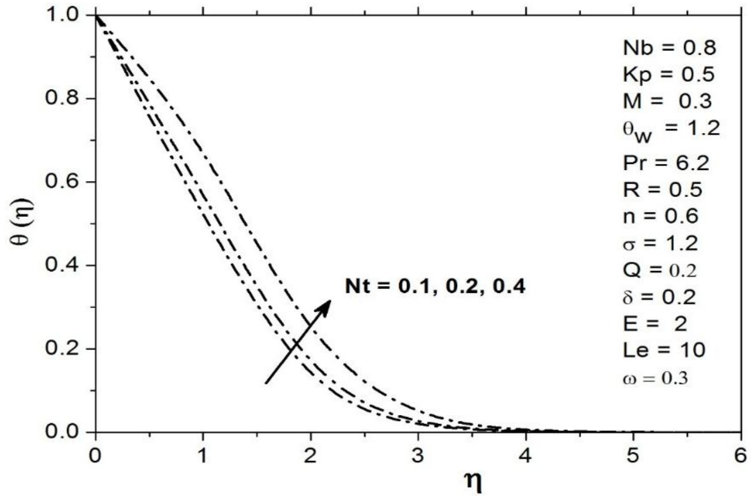

Figure 15: Temperature profile for thermophoresis parameter.

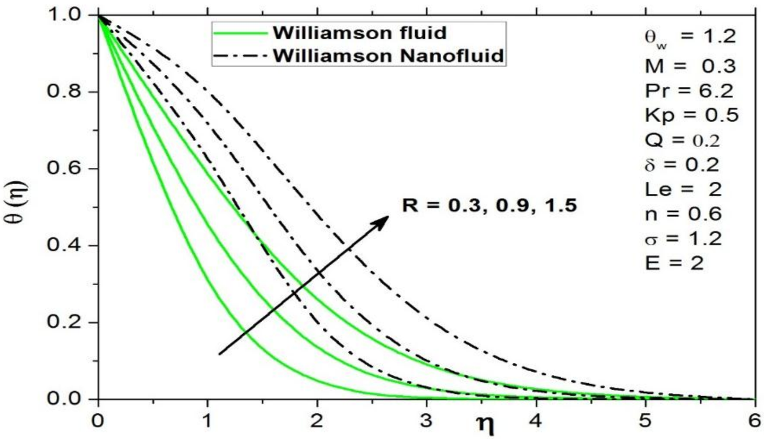

Figure 16: Temperature profile for radiation parameter.

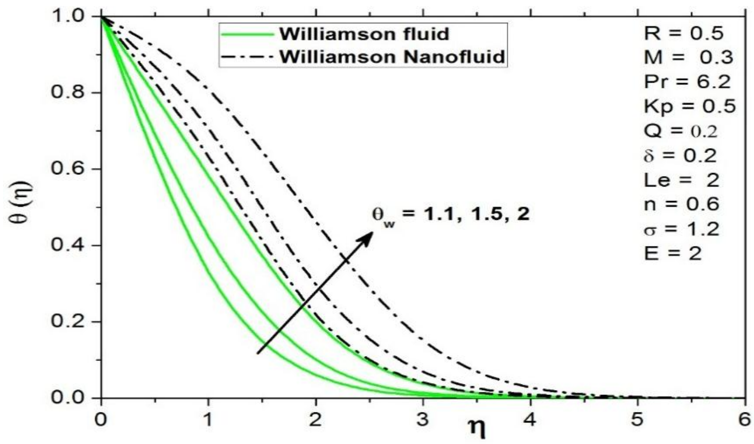

Figure 17: Temperature profile for temperature ratio parameter.

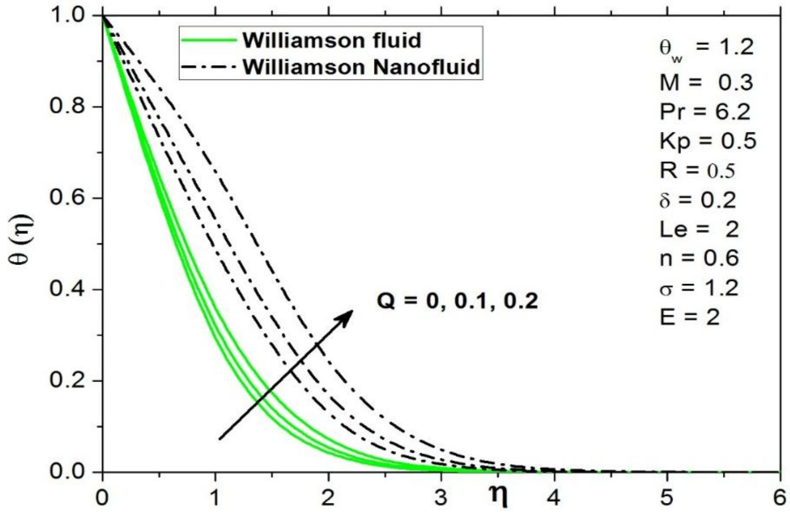

Figure 18: Temperature profile for heat source parameter.

Concluding Remarks

Our study delved into the impact of nanoparticles on the magnetohydrodynamic flow of a Williamson fluid over a permeable exponential stretched surface. We meticulously compared scenarios with and without nanoparticles in the Williamson fluid, while also considering the effects of solar radiation, chemical reaction, and activation energy. Through our investigation, several key findings emerged:

- The thermal and volume fraction boundary layer thickness increases in case of nanoliquid model (Williamson nanoliquid) than ordinary fluid model (Williamson fluid) case.
- The thermophoresis and Brownian motion aspects are developed the thermal boundary layer thickness.
- Liquid velocity reduces at the medium in presence of porous.
- The mass transfer rate is more in Williamson nanofluid case than Williamson fluid but quit opposite behaviour can be observed in heat transfer process.
- Generates more heat into the liquid flow through radiation phenomena, in fact better temperature is achieved.
- Enhanced the concentration profile for superior activation energy.
- Results of non-Newtonian fluid can be recovered when $Nb = Nt = 0$.

Tables and Graphs

Table 1: Numerical values of $C_f Re_x^{0.5}$, $Nu_x/(2Re_x)^{0.5}$ and $Sh_x/(2Re_x)^{0.5}$ for different values of the various parameters.

E	Le	σ	δ	R	Tw	Q	Williamson fluid		Williamson nanofluid	
							$\frac{Nu_x}{(2Re_x)^{0.5}}$	$\frac{Sh_x}{(2Re_x)^{0.5}}$	$\frac{Nu_x}{(2Re_x)^{0.5}}$	$\frac{Sh_x}{(2Re_x)^{0.5}}$
2	2	1.2	0.2	0.5	1.2	0.2	1.307121	1.038949	-0.09822	1.143927
0.5							1.307121	1.545418	-0.07864	1.669161
1							1.307121	1.326286	-0.08749	1.448424
2							1.307121	1.038949	-0.09822	1.143927
	0.5						1.307121	0.451286	0.068688	0.512258
	1						1.307121	0.680761	-0.05614	0.77143
	2						1.307121	1.038949	-0.09822	1.143927
		0.4					1.307121	0.87112	-0.10586	0.94655
		0.8					1.307121	0.958534	-0.10194	1.050932
		1.2					1.307121	1.038949	-0.09822	1.143927
			0.2				1.307121	1.038949	-0.09822	1.143927
			0.4				1.307121	1.102506	-0.09049	1.229458
			0.6				1.307121	1.167257	-0.0836	1.313714
				0.5			1.186052	1.038949	-0.09822	1.122410
				1			1.301606	1.046936	-0.07523	1.127566
				1.5			1.307121	1.053237	-0.06756	1.143927
					1.2		1.307121	1.038949	-0.09822	1.113323
					1.5		1.362698	1.044268	-0.03335	1.127951
					2		1.365862	1.053999	0.041915	1.143927
						0.1	1.679188	1.03513	0.253448	1.094415
						0.2	1.307121	1.038949	-0.09822	1.143927
						0.25	1.076933	1.041527	-0.3391	1.176248

References

[1] R. V. Williamson, "The flow of pseudoplastic materials," Industrial & Engineering Chemistry, Vol. 21, no. 11, pp. 1108-1111, 1929. DOI: 10.1021/ie50239a035

[2] D.V. Lyubimov, and A. V. Perminov, "Motion of a thin oblique layer of a pseudoplastic fluid," Journal of Engineering Physics and Thermophysics, Vol. 75, no. 4, pp. 920-924, 2002. DOI: 10.1023/A:1020371203799.

[3] S. Nadeem, S. Ashiq, and M. Ali, "Williamson fluid model for the peristaltic flow of chyme in small intestine," Mathematical Problems in Engineering, Vol. 2012, no. 1, pp. 479087, 2012. DOI: 10.1155/2012/479087

[4] M. Dhivya K. Vajravelu, Heat transfer characteristics of a Williamson fluid flow through a variable porosity regime, Int. J. Ambient Energy., 44(1) (2023).

[5] S.O. Salawu, "Stagnation-point flow of Williamson fluid along a stretched plate with convective thermal condition and activation energy," International Journal of Applied Mechanics and Engineering, Vol. 28, no. 3, 2023. DOI: 10.59441/ijame/172900.

[6] M.M. Rashidi, N. Vishnu Ganesh, A.K. Abdul Hakeem, and B. Ganga, "Buoyancy effect on MHD flow of nanofluid over a stretching sheet in the presence of thermal radiation," Journal of Molecular liquids, Vol. 198, pp. 234-238, 2014. DOI: 10.1016/j.molliq.2014.06.037.

[7] K. Das, P. R. Duari, and P.K. Kundu, "Nanofluid flow over an unsteady stretching surface in presence of thermal radiation," Alexandria engineering journal, Vol. 53, no. 3, pp. 737-745, 2014. DOI: 10.1016/j.aej.2014.05.002

[8] B. Mahanthesh, B. J. Gireesha, S. A. Shehzad, A. Rauf, and P.B. Sampath Kumar, "Nonlinear radiated MHD flow of nanoliquids due to a rotating disk with irregular heat source and heat flux condition," Physica B: Condensed Matter, Vol. 537, pp. 98-104, 2018. DOI: 10.1016/j.physb.2018.02.009

[9] M.I. Khan, T. Hayat, M. Imran Khan, M. Waqas, and A. Alsaedi, "Numerical simulation of hydromagnetic mixed convective radiative slip flow with variable fluid properties: a mathematical model for entropy generation," Journal of Physics and Chemistry of Solids, Vol. 125, pp. 153-164, 2019. DOI: 10.1016/j.jpcs.2018.10.015.

[10] Y.D. Reddy, B. Shankar Goud, Ali J. Chamkha, and M. Anil Kumar, "Influence of radiation and viscous dissipation on MHD heat transfer Casson nanofluid flow along a nonlinear stretching surface with chemical reaction," Heat Transfer, Vol. 51, no. 4, pp. 3495-3511, 2022. DOI: 10.1002/htj.22460

[11] D. Pal, and H. Mondal, "Influence of temperature-dependent viscosity and thermal radiation on MHD forced convection over a non-isothermal wedge," Applied Mathematics and Computation, Vol. 212, no. 1, pp. 194-208, 2009. DOI: 10.1016/j.amc.2009.02.013.

[12] O.D. Makinde, "Chemically reacting hydromagnetic unsteady flow of a radiating fluid past a vertical plate with constant heat flux," Zeitschrift für Naturforschung A, Vol. 67, no. 5, pp. 239-247, 2012. DOI: 10.5560/zna.2012-0014

[13] S.A. Shehzad, T. Hayat, A. Alsaedi, and M. A. Obid. "Nonlinear thermal radiation in three-dimensional flow of Jeffrey nanofluid: a model for solar energy," Applied Mathematics and Computation, Vol. 248 pp. 273-286, 2014. DOI: 10.1016/j.amc.2014.09.091

[14] C.S.K. Raju, S. M. Ibrahim, S. Anuradha, and P. Priyadharshini, "Bio-convection on the nonlinear radiative flow of a Carreau fluid over a moving wedge with suction or injection," The European Physical Journal Plus, Vol. 131, pp. 1-16, 2016. DOI: 10.1140/epjp/i2016-16409-7

[15] K. Sajjan, N.A. Shah, N.A. Ahammad, C.S.K. Raju, M.D. Kumar, W. Weera, "Nonlinear Boussinesq and Rosseland approximations on 3D flow in an interruption of Ternary nanoparticles with various shapes of densities and conductivity properties," AIMS Math, Vol. 7, no. 10, pp. 18416-18449, 2022. DOI: 10.3934/math.20221014.

[16] B.J. Gireesha, S. Manthesha, F. Almeida, P. Mallikarjun, "Flow of magnetized Powell-Eyring fluid in microchannel exposed to non-linear radiation and constricted to slip regime by varying viscosity," International Journal of Modelling and Simulation, pp. 1-14, 2023. DOI:10.1080/02286203.2023.2216049.

[17] K. Anantha Kumar, A.C. Venkata Ramudu, V. Sugunamma, N. Sandeep, "Effect of non-linear thermal radiation on MHD Casson fluid flow past a stretching surface with chemical reaction," International Journal of Ambient Energy, Vol. 43, no. 1, pp. 8400-8407, 2022. DOI:10.1080/01430750.2022.2097947.

[18] M. Ismail, D.M. Gururaj, "Numerical investigation on nonlinear radiative magneto hydrodynamics hybrid nanofluid flow past a stretching cylinder embedded in porous medium," Journal of Nanofluids, Vol. 12, no. 3, pp. 809-818, 2023. DOI: 10.1166/jon.2023.1962

[19] S. Mukhopadhyay, K. Bhattacharyya, "Unsteady flow of a Maxwell fluid over a stretching surface in presence of chemical reaction," Journal of the Egyptian Mathematical Society, Vol. 20, no. 3, pp. 229-234, 2012. DOI: 10.1016/j.joems.2012.08.019

[20] T. Hayat, M. Rashid, M. Imtiaz, A. Alsaedi, "MHD convective flow due to a curved surface with thermal radiation and chemical reaction," Journal of Molecular Liquids, Vol. 225 pp. 482-489, 2017. DOI: 10.1016/j.molliq.2016.11.096

[21] J.C. Umavathi, M.A. Sheremet, S. Mohiuddin, "Combined effect of variable viscosity and thermal conductivity on mixed convection flow of a viscous fluid in a vertical channel in the presence of first order chemical reaction," European Journal of Mechanics-B/Fluids, Vol. 58, pp. 98-108, 2016. DOI: 10.1016/j.euromechflu.2016.04.003

[22] M. Mustafa, J.A. Khan, T. Hayat, A. Alsaedi, "Buoyancy effects on the MHD nanofluid flow past a vertical surface with chemical reaction and activation energy," International Journal of Heat and Mass Transfer, Vol. 108, pp. 1340-1346, 2017. DOI: 10.1016/j.ijheatmasstransfer.2017.01.029.

[23] A. Majeed, A. Zeeshan, R. Ellahi, "Chemical reaction and heat transfer on boundary layer Maxwell Ferro-fluid flow under magnetic dipole with Soret and suction effects," Engineering science and technology, an international journal, Vol. 20, no. 3, pp. 1122-1128, 2017. DOI: 10.1016/j.jestch.2016.11.007

[24] M. Nadeem, I. Siddique, I. Saif Ud Din, F.A. Awwad, Emad AA Ismail, H. Ahmad, "Impact of chemical reaction on Eyring–Powell fluid flow over a thin needle with nonlinear thermal radiation," Scientific Reports, Vol. 13, no. 1, pp. 21401, 2023. DOI: 10.1038/s41598-023-48400-1.

[25] S.U.S. Choi, “Enhancing thermal conductivity of fluids with nanoparticles, developments and applications of non-Newtonian flows,” ASME, FED, MD, Vol. 1995, no. 231, pp. 99-I05, 1995.

[26] K. Muhammad, T. Hayat, A. Alsaedi, "Numerical study of Newtonian heating in flow of hybrid nanofluid (SWCNTs+ CuO+ Ethylene glycol) past a curved surface with viscous dissipation," Journal of Thermal Analysis and Calorimetry, Vol. 143, pp. 1291-1302, 2021. DOI: 10.1007/s10973-020-10196-x.

[27] M.I. Khan, K. Muhammad, T. Hayat, S. Farooq, A. Alsaedi, "Numerical simulation for Darcy-Forchheimer flow of carbon nanotubes due to convectively heated nonlinear curved stretching surface," International Journal of Numerical Methods for Heat & Fluid Flow, Vol. 29, no. 9, pp. 3290-3304, 2019. DOI: 10.1108/HFF-01-2019-0016.

[28] A. Ali, R.N. Jana, S. Das, "Radiative CNT-based hybrid magneto-nanoliquid flow over an extending curved surface with slippage and convective heating," Heat Transfer, Vol. 50, no. 3, pp. 2997-3020, 2021. DOI: 10.1002/htj.22015.

[29] B. Kumbhakar, S. Nandi, A.J. Chamkha, "Unsteady hybrid nanofluid flow over a convectively heated cylinder with inclined magnetic field and viscous dissipation: a multiple regression analysis," Chinese Journal of Physics, Vol. 79, pp. 38-56, 2022. DOI: 10.1016/j.cjph.2022.07.003.

[30] A. Ali, S. Malik, M. Awais, A. S. Alqahtani, M.Y. Malik, "MHD peristaltic flow of hybrid nanomaterial between compliant walls with slippage and radiation," Journal of Molecular Liquids, Vol. 393, pp. 123619, 2024. DOI: 10.1016/j.molliq.2023.123619.

[31] P.L. Pavan Kumar, B.J. Gireesha, P. Venkatesh. "Impact of trihybrid nanofluid on the transient thermal performance of inclined dovetail fin with emphasis on internal heat generation," The European Physical Journal Plus, Vol. 139, no. 1, pp. 1-18, 2024. DOI: 10.1140/epjp/s13360-023-04848-8.

[32] S. Manjunatha, V. Puneeth, B. J. Gireesha, A.J. Chamkha, "Theoretical study of convective heat transfer in ternary nanofluid flowing past a stretching sheet," Journal of Applied and ComputationalMechanics,Vol.8,no.4,pp.1279-1286,2022. Doi: 10.22055/jacm.2021.37698.3067.

[33] S.H. Godasiaei, A.J. Chamkha, "Advancing heat transfer modeling through machine learning: A focus on forced convection with nanoparticles," Numerical Heat Transfer, Part A: Applications, pp. 1-23, 2023. DOI:10.1080/10407782.2023.2299734

[34] W. Shao, M.K. Nayak, R. Ali, S. Nazari, A.J. Chamkha, "Simultaneous numerical examination of thermal and entropy characteristics of Al2O3–H2O nanofluid within a porous diamond-shaped container with a⊥-shaped obstacle," Case Studies in Thermal Engineering, Vol. 54, pp. 104059, 2024. DOI: 10.1016/j.csite.2024.104059